Published in final edited form as:
Biochemistry. 2010 September 14; 49(36): 7902–7912. doi:10.1021/bi1009375.

Oxidation Reactions Performed by Soluble Methane Monooxygenase Hydroxylase Intermediates H_{peroxo} and Q Proceed by Distinct Mechanisms†

Christine E. Tinberg and **Stephen J. Lippard***
Department of Chemistry, Massachusetts Institute of Technology, Cambridge, Massachusetts 02139

Abstract

Soluble methane monooxygenase is a bacterial enzyme that converts methane to methanol at a carboxylate-bridged diiron center with exquisite control. Because the oxidizing power required for this transformation is demanding, it is not surprising that the enzyme is also capable of hydroxylating and epoxidizing a broad range of hydrocarbon substrates in addition to methane. In this work we took advantage of this promiscuity of the enzyme to gain insight into the mechanisms of action of H_{peroxo} and Q, two oxidants that are generated sequentially during the reaction of reduced protein with O_2. Using double-mixing stopped flow spectroscopy, we investigated the reactions of the two intermediate species with a panel of substrates of varying C–H bond strength. Three classes of substrates were identified according to the rate-determining step in the reaction. We show for the first time that an inverse trend exists between the rate constant of reaction with H_{peroxo} and the C–H bond strength of the hydrocarbon examined for those substrates in which C–H bond activation is rate-determining. Deuterium kinetic isotope effects revealed that reactions performed by Q, but not H_{peroxo}, involve extensive quantum mechanical tunneling. This difference sheds light on the observation that H_{peroxo} is not a potent enough oxidant to hydroxylate methane, whereas Q can perform this reaction in a facile manner. In addition, the reaction of H_{peroxo} with acetonitrile appears to proceed by a distinct mechanism in which a cyanomethide anionic intermediate is generated, bolstering the argument that H_{peroxo} is an electrophilic oxidant and operates via two-electron transfer chemistry.

Soluble methane monooxygenase (sMMO[1]) isolated from *Methylococcus capsulatus* (Bath) catalyzes the selective conversion of methane to methanol at room temperature and atmospheric pressure (1). This difficult transformation requires the coordinated effort of three protein components: a dimeric hydroxylase (MMOH) that houses two copies of a diiron catalytic center, a reductase (MMOR) that accepts electrons from NADH and transfers them to the hydroxylase, and a regulatory protein (MMOB) that couples electron

†This work was funded by grant GM032134 from the National Institute of General Medical Sciences. CET thanks the NIH for partial support under Interdepartmental Biotechnology Training Grant T32 GM08334.

* To whom correspondence should be addressed. lippard@mit.edu. Telephone: (617) 253-1892. Fax: (617) 258-8150..

SUPPORTING INFORMATION Figures S1-S9 as described in the text and Figure S10 showing the concentration-dependences of rate constants for reaction of Q with CH_3CH_2CHO (PDF). This material is available free of charge via the Internet at http://pubs.acs.org.

[1]Abbreviations: sMMO, soluble methane monooxygenase; MMOH, hydroxylase protein of sMMO; MMOB, regulatory component of sMMO; MMOR, reductase component of sMMO; H_{ox}, di(μ-hydroxo)diiron(III) resting state of MMOH; H_{red}, diiron(II) form of MMOH; P*, first peroxodiiron(III) intermediate observed upon reaction of $MMOH_{red}$ with O_2; H_{peroxo}, second peroxodiiron(III) intermediate observed upon reaction of $MMOH_{red}$ with O_2; Q, di(μ-oxo)diiron(IV) species observed during reaction of $MMOH_{red}$ with O_2; Q*, oxygenated-iron intermediate formed as a result Q decay in the absence of hydrocarbon substrate; BDE, bond dissociation energy; IP, ionization potential.

transfer to substrate oxidation in a complex manner. Although its physiologically relevant substrate is methane, sMMO can oxidize a wide variety of substrates including alkanes, alkenes, alkynes, aromatics, heterocycles, halogenated compounds, and small inorganic molecules such as carbon monoxide (2-4). Substrates range in size from methane to the relatively large radical clock probe 2,2-diphenylmethylcyclopropane (5). The oxidation reactions of MMOH proceed by multiple mechanisms including hydroxylation, epoxidation, and oxygen atom transfer depending on the substrate.

The catalytic cycle of MMOH in the presence of MMOB is well established (Scheme 1). In the first step, the diiron(III) resting state of H_{ox} is reduced to an O_2-reactive diiron(II) species, H_{red}, by two electrons originating from NADH. Following reaction of H_{red} with dioxygen, the first intermediate observed spectroscopically is P*, a putative peroxodiiron(III) species (6, 7). The Mössbauer spectrum of P* is consistent with two antiferromagnetically coupled high-spin iron(III) centers with similar coordination geometries (8). P* rapidly converts to H_{peroxo}, a distinct peroxodiiron(III) species characterized by optical bands at 420 and 725 nm, in a proton-driven process (7, 9). Because of similarities in the spectroscopic parameters of P* and H_{peroxo}, these two intermediates are expected to have similar iron-oxygen cores (7). Based on analogy to peroxo intermediates from other diiron proteins (10-14) and theoretical calculations (15), H_{peroxo} is most likely a gauche μ-1,2-peroxo species; however, a nonplanar μ-η^2:η^2 peroxide diiron(III) binding mode has also been proposed (16-18).

In the absence of substrate, H_{peroxo} decays to intermediate Q in a second proton-driven process (7, 9). Q features a broad absorption band centered at 420 nm (8, 19, 20). Spectroscopic characterization of this intermediate revealed that is a di(μ-oxo)diiron(IV) cluster with a diamagnetic ground state due to antiferromagnetic coupling between the iron atoms (8, 19, 21), and analysis by EXAFS spectroscopy revealed a short Fe–Fe distance of 2.46 Å (22). The reactivity of Q with various substrates has been extensively investigated and it is generally accepted that this species is responsible for methane oxidation (6, 23, 24). Studies employing high-level density functional theory suggested that the hydroxylation of methane by Q is initiated by a proton-coupled outer-sphere electron transfer from a C–H σ bond in methane through the bridging oxygen atom to one of the iron atoms, generating a transiently bound, substrate-derived radical intermediate (Scheme 2a) (25). Although the rate-determining step in the reaction mechanism is thought to involve hydrogen atom transfer, multiple studies have revealed that there is no correlation between the rate constant for reaction of a given substrate with Q and the homolytic bond dissociation energy (BDE) of that substrate. These findings indicate that that there are aspects of the reaction mechanisms that are still incompletely understood. In the absence of substrate, Q decays slowly to H_{ox} by a mechanism that proceeds through a recently identified intermediate Q* of unknown composition (7).

Most of the literature on the hydroxylation mechanisms of MMOH has focused on reactions of Q because this species is responsible for methane oxidation, but recent evidence suggests that H_{peroxo} also reacts with hydrocarbon substrates (20, 26). Early evidence that the H_{peroxo} and Q intermediate species of MMOH operate as distinct oxidants was provided by reports that different product distributions were obtained for certain substrates depending on whether the oxidized form of the enzyme was activated with NADH and O_2 or with hydrogen peroxide in the absence of MMOB (27, 28). More recently, double-mixing stopped-flow spectroscopy demonstrated that the rate constant for H_{peroxo} decay is accelerated in the presence of the electron-rich substrates propylene, ethyl vinyl ether, and diethyl ether (20, 26). Both ethyl vinyl ether and diethyl ether react more rapidly with H_{peroxo} than with Q under pre-steady-state conditions. A comparison of rate constants for these reactions indicates that H_{peroxo} is a more electrophilic oxidant than Q. Based on these

results, we suggested that the mechanism of oxidation by H_{peroxo} involves an initial two-electron transfer event from substrate to form a transient, substrate-derived cationic species that rebounds with the two-electron reduced iron core to form H_{ox} and an epoxide or hydroxylated product (Scheme 2b) (26). The proposed mechanism is also supported by the presence of cation-derived products observed in the steady state reactions of radical clock substrate probes with sMMO (29-32).

To elaborate on the mechanisms of substrate reactivity in MMOH, we conducted a systematic study investigating structure-activity relationships for hydroxylation reactions promoted by H_{peroxo} and Q and describe the results in this report. These experiments, enabled by the promiscuity of the enzyme, demonstrate that H_{peroxo} and Q interact and react with different substrates by distinct mechanisms in a manner that depends largely on the molecular dipole of the substrate. Three classes of substrates are defined: (i) those for which substrate binding is rate-determining at all substrate concentrations; (ii) those for which C–H bond cleavage is rate-determining at all substrate concentrations; and (iii) those for which the rate-determining step is dependent on substrate concentration. An analysis of the substrates belonging to the three classes is presented and mechanistic findings regarding the reactions of the two intermediates are discussed.

MATERIALS AND METHODS

General Considerations

The hydroxylase (MMOH) enzyme was purified from *Methylococcus capsulatus* (Bath) as described previously (26). Protein obtained had a specific activity at 45 °C in the range of 300-450 mU/mg, as measured for propylene oxidation at 45 °C (20). Iron content was determined using the ferrozine colorimetric iron assay and ranged from 3.4-4.0 iron atoms per protein dimer (20). The regulatory (MMOB) and reductase (MMOR) proteins were expressed recombinantly in *E. coli* and purified as described elsewhere (33, 34). The buffer system employed in all experiments was 25 mM potassium phosphate pH 7.0. Distilled water was deionized with a Milli-Q filtering system. Other reagents were purchased from Sigma Aldrich and were used as received.

Stopped-Flow Optical Spectroscopy

Kinetic experiments were performed on a Hi-Tech Scientific (Salisbury, UK) SF-61 DX2 stopped-flow spectrophotometer as described in detail elsewhere (20). Briefly, a solution of 200 μM MMOH and 400 μM MMOB was prepared in 25 mM potassium phosphate buffer, pH 7.0. The hydroxylase was reduced with excess sodium dithionite using stoichiometric methyl viologen as a redox mediator. Excess reducing agent was removed by dialysis.

Double-mixing stopped-flow experiments were performed by rapidly mixing the reduced protein solution with O_2-saturated buffer. After a specified time delay corresponding to the maximal accumulation of H_{peroxo} or Q, substrate-containing buffer was introduced in a second push to initiate the reaction and trigger the start of data collection. The delay times between the first and second mixing events were determined by monitoring the reaction kinetics at 420 and 720 nm in the absence of substrate, 12 s for Q and 2 s for H_{peroxo} (7). All experiments were performed at 4 °C using a circulating water bath. The concentration of MMOH:2B in the sample cell after mixing was 50 μM in all experiments. Data monitoring the reactions of Q and H_{peroxo} were collected at 420 and 720 nm, respectively, using a photomultiplier tube. Data were collected in duplicate or triplicate, using different protein preparations for each experiment. Data were collected under control of the KinetAsyst 3 (Hi-Tech Scientific) and Kinetic Studio (Hi-Tech Scientific) software.

All substrates used in double-mixing stopped-flow experiments were purchased from Sigma Aldrich and used as received. Substrate purity was assessed by ^{1}H-NMR spectroscopy. Substrate solutions were prepared in volumetric flasks containing a weighed amount of material. For volatile liquid substrates, the volumetric flask was fitted with a rubber septum and the substrate was injected through the septum into buffer maintained at 4 °C. Protein stability was not compromised in the presence of any of the substrates at the concentrations employed in the experiments, as noted optically by the absence of protein precipitation over the course of 30 min incubation with substrate.

Data Analysis

Data analyses were performed with KinetAsyst 3 (Hi-Tech Scientific) and/or Kinetic Studio (Hi-Tech Scientific) and/or KaleidaGraph v 3.51 (Synergy Software) software, and the programs provided the same results in all cases. In fitting primary data, only results that displayed an R^2 value of 0.998 or greater were deemed acceptable. Data were evaluated on the basis of this value, the fit residuals, and the parameter errors.

Data monitoring Q decay in the presence of substrate were fit well to a single exponential function, as described previously (Figure S1a, Supporting Information) (6, 20, 23, 26). This procedure is justified by the fact that Q represents most of the active diiron centers (89%) at the age time employed in these experiments (7). Additionally, Q reacts with all substrates employed, presumably to form H_{ox} and product; therefore, kinetic terms representing Q* formation and decay did not have to be included in any fits.

Data monitoring H_{peroxo} decay in the presence of substrate were fit well by a two-exponential function, as described previously (Figure S1b) (26). At 2 s, the age time employed in the experiments, the active diiron sites comprise 22% P*, 51% H_{peroxo}, and 26% Q (7); therefore, it is necessary to account for a significant population of Q that is present in the reaction mixture. For most substrates it was sufficient to fix the value of k_{obs2} at that measured independently in experiments monitoring substrate-promoted Q decay. However, for some substrates satisfactory fits were not obtained when k_{obs2} was fixed. These substrates include CH_3CHO and CH_3CH_2CHO at concentrations above ~10 mM. In both cases, k_{obs2} was smaller than the value of substrate-promoted Q decay observed independently in experiments probing reaction of Q. This finding is most likely due to optical contributions from H_{peroxo} to Q conversion, which are not explicitly accounted for in the exponential fitting model and can arise if a population of H_{peroxo} decays by conversion to Q rather than by reaction with substrate. These processes should have a more dominant effect on the rate constant measured for Q decay when reaction with H_{peroxo} is rapid, because substrate-promoted H_{peroxo} decay separates in time from H_{peroxo} to Q conversion and substrate-promoted Q decay. This phenomenon causes Q formation to be incorporated into the exponential term for Q decay, thereby making k_{obs2} appear smaller than it is when the rate constant for reaction with subsrate (k_{obs} in Q experiments) is larger than that of H_{peroxo} to Q conversion. For all other substrates, this problem did not arise because the rate constant for reaction with H_{peroxo} was not significantly faster than that for Q, except for CD_3NO_2. For this substrate, reactions with H_{peroxo} were least 100 times faster than those with Q at each substrate concentration when $[CD_3NO_2] > 200$ mM. At these concentrations, the exponential phases corresponding to H_{peroxo} and Q decay were well separated when a 2 s age time was employed. These data were fit well by truncating and analyzing each phase separately using independent single exponential processes (Figure S2).

RESULTS AND DISCUSSION

Soluble methane monooxygenase is a remarkable enzyme system that selectively oxidizes methane to methanol even in the presence of cellular metabolites and active site amino acid

residues having much weaker C–H bonds. Studies from our lab suggest that *two* sequential oxidants in the system, H_{peroxo} and Q, are responsible for its broad reactivity with a variety of substrates. To characterize the reactive properties of this enzyme, we undertook a systematic study employing single- and double-mixing stopped-flow optical spectroscopy to demonstrate conclusively that H_{peroxo} is reactive and to monitor the reactions of the oxygenated-iron intermediates with substrates of varying C–H bond strength. Structure-reactivity correlations in enzyme systems are often hindered by the substrate binding specificities; however, the broad substrate reactivity pattern of MMOH enabled us to perform such a study in this system.

Single-Mixing Stopped Flow Studies – Proof that H_{peroxo} is a Hydrocarbon Oxidant

The evidence that H_{peroxo} reacts with substrates is substantial (20, 26). However, to further evaluate this hypothesis we used the unique approach of investigating the reaction of $MMOH_{red}$ with a mixture of O_2 and a substrate known to react with H_{peroxo} in the presence of 2 equiv of MMOB by single-mixing stopped-flow spectroscopy. The substrate chosen for these studies was CH_3CH_2CHO, because this aldehyde was identified as a substrate that reacts rapidly with H_{peroxo} in double-mixing studies (vide infra). Similar studies performed in the presence of methane, which reacts with Q but not H_{peroxo}, demonstrated a rise and decay in absorbance at 420 nm and high substrate concentrations. Because Q does not accumulate under these conditions, the observed absorbance profile was attributed solely to accumulation of H_{peroxo} and its precursor, P*, both of which absorb at this wavelength (7). We reasoned that if H_{peroxo} and/or P*, which is believed to have a similar oxygen-iron core as H_{peroxo} and therefore might exhibit similar reactivity properties, react with CH_3CH_2CHO then we should observe no rise and decay in absorbance at 420 nm when the concentration of substrate is high enough to prevent accumulation of these species due to rapid reaction. If no reaction occurred, the results would be identical to those for the reaction with methane (7).

Reactions of $MMOH_{red}$ with a mixture of O_2 and CH_3CH_2CHO in the presence of 2 equiv of MMOB are shown in Figure 1 (420 nm) and Figure S3 (720 nm). In the absence of substrate, the time-dependent formation and decay of intermediates P*, H_{peroxo}, and Q are responsible for a rise and decay in absorbance at 420 nm (Figure 1a). As the substrate concentration was increased, the amplitude of this signal diminished and the time of maximal accumulation decreased, indicating that components contributing to the signal are depleted faster than in the absence of substrate. At the highest substrate concentrations employed, this rise and decay in absorbance was not observed because the intermediates do not accumulate. At these concentrations the time-dependent profiles did not change significantly with increasing substrate concentration. Only a slight decay in absorbance was seen, presumably due to decay of H_{red} (Figure 1b). Data collected at 214.9 mM CH_3CH_2CHO, the highest substrate concentration employed, fit well to a single exponential decay with rate constant $5.6 \pm 0.1\ s^{-1}$ at 420 nm and 720 nm (Figures 1b and Figure S3b). This value is within error of that measured previously for H_{red} decay/P* formation (7), confirming conclusively that P* and possibly H_{peroxo} do not accumulate under these conditions. These observations are distinct from those probing the reaction of the enzyme with methane, and reactivity with P* and probably H_{peroxo} is the only plausible explanation for these results.

Double-Mixing Stopped Flow Studies – Delineating the Reactivities of Diiron(III) Peroxo vs Diiron(IV) Oxo Intermediates

To gain insight into the reaction mechanisms of H_{peroxo}/P* and Q with substrates, we used double mixing stopped-flow spectroscopy to generate H_{peroxo} or Q and then we introduced a substrate of interest and followed the ensuing optical events. Previous reports have taken the

rate constant for H_{peroxo} or Q decay in the presence of a given substrate as a measure of the rate at which the intermediate of interest reacts with that substrate (6, 8, 19, 20, 23, 26, 35). A definitive study employing stopped-flow Fourier transform infrared spectroscopy confirmed that this method appropriately describes the rate of reaction with substrate; the rate constant for Q decay, measured by optical spectroscopy, in the presence of the alternative substrate CD_3NO_2 was the same at that for substrate consumption, measured by FT-IR spectroscopy (36). A similar conclusion was reached in an early study employing nitrobenzene as a substrate (37). These findings allowed us to employ stopped-flow spectroscopy in order to measure the decay rate constants for H_{peroxo} and Q in the presence of various substrates in order to gain information about the reactions of these intermediates.

Reactions of H_{peroxo} and Q monitored at 4 °C and pH 7.0 in this manner fit into one of three categories based on the nature of the rate-determining step in the reaction, as determined by the dependence of the rate constant for intermediate decay (k_{obs}) on substrate concentration and by the effects of substrate deuteration (Table 1). Substrates were classified according to the following criteria: (i) linear dependence of k_{obs} on substrate concentration and a kinetic isotope effect (KIE), k_H/k_D, of unity; (ii) linear dependence of k_{obs} on substrate concentration and KIE > 1; and (iii) hyperbolic dependence of k_{obs} on substrate concentration (23, 38).

Class I Reactions

Reactions of Q with Class I substrates display a linear dependence of rate on substrate concentration and a KIE near unity, results suggesting that for these substrates C–H bond breaking is not rate-determining (Table 2). Rather, substrate access to the active site appears to determine the kinetics, even at high substrate concentrations. Second order rate constants for these reactions were determined by fitting the data to eq 1, where k_{obs} is the observed rate constant at a given substrate concentration, k_0 is the rate constant of intermediate decay in the absence of substrate, and k is

$$k_{obs} - k_0 = k[S] \quad (1)$$

the second-order rate constant for the overall reaction. Class I substrates for Q include only the alcohols methanol (Figure 2) and ethanol (Figure S4), where the former reaction yields formaldehyde exclusively (23). An additional substrate that falls into this class for reaction with Q is ethane (39).

For Class I substrates, the approach to the active site, rather than C–H bond activation, might be rate-determining. In MMOH, hydrocarbon substrates are thought to access the active site diiron center via a series of five hydrophobic cavities that feature only a few polar amino acid side chains (40). Favorable hydrophobic interactions between nonpolar substrates such as ethane and the hydrophobic side chains of residues in the active site pocket and possibly those that line the protein cavities could prevent rapid access to the active site. High-level QM/MM density functional theory studies probing the reaction of Q with ethane support this mechanism (41). In the case of alcohols, *favorable* hydrogen-bonding or van der Waals interactions between the substrate hydroxyl group and polarizable residues in the active site and possibly the other cavities could lead to the observed effect by stabilizing the transition state for C–H bond activation relative to that for substrate binding. In this manner, such interactions could lower the barrier height for the former process and render the latter rate-determining at all substrate concentrations. Computational studies predict that this type of mechanism is operative during the reaction of methanol with Q (41). During this reaction, the active site cavity orients the substrate in such a way that a hydrogen bond forms between the alcohol group and the backbone carbonyl of an active site glycine

reside, G113, stabilizing the transition state for C–H bond activation relative to that of substrate binding (41). A similar interaction is expected to occur with ethanol.

Surprisingly, class I type behavior was not observed for H_{peroxo} among the substrates employed in the study. Even methanol and ethanol, class I substrates of Q, displayed KIEs greater than unity for reaction with H_{peroxo} (vide infra). These findings reveal that there is a disparity in the manner that the two intermediates react with these substrates, a conclusion derived from differences in the rate-determining steps of the reaction. For reactions of alcohols with H_{peroxo}, the rate-determining step is C–H bond activation instead of substrate binding. It is likely that structural changes occur at the diiron center during conversion of H_{peroxo} to Q, which might alter the manner by which substrates can approach the active site, thereby influencing the rate-determining step. Of relevance is the finding that significant KIEs were observed in pre-steady state reactions of ethane with Q when mutant forms of MMOB were employed, but not when wild-type MMOB was used (39, 42). Although these results do not specifically inform us about the differential reactivity of the two MMOH intermediates, they suggest that geometric differences at the active site in the MMOH/MMOB complex, in this case imparted by MMOB amino acid substitutions, can alter the relative thermodynamics of the substrate binding and C–H bond activation steps. Differential steric constraints imposed by the geometries of the iron-oxygen intermediate species could have a similar effect on the reactions. For the reaction of methanol with H_{peroxo}, a favorable interaction of the alcohol group with the carbonyl of G113 to lower the barrier height for reaction with Q (vide supra) might not provide the same stabilizing force for reaction with H_{peroxo} due to stereochemical differences, leading to the observed effects.

Class II Reactions

Reactions of H_{peroxo} and Q with Class II substrates depend linearly on substrate concentration and have KIE > 1, suggesting that C–H activation is fully or partially rate-determining for these substrates, even at low substrate concentrations. For these substrates, there does not appear to be a discrete substrate-binding step, and the kinetics best resemble those for a small molecule catalyst rather than an enzyme, which requires a traditional Michaelis-Menten treatment. Diffusion to the active site is rapid and in all cases faster than the C–H bond activation chemistry. For H_{peroxo}, these substrates include methanol (Figure S5), ethanol (Figure 3), and diethyl ether (26) (Table 3). For Q, only diethyl ether (26) and methane (6, 20, 23) exhibit such behavior.

The second-order rate constants for reaction of class II substrates with H_{peroxo} correlate with the strength of the weakest C–H bond (Table 4). For diethyl ether, which has two types of C–H groups, the weakest C–H bond is the one that becomes hydroxylated during steady state assays (2, 26). Substrates with the lowest homolytic (D(RH)) and heterolytic ($D(R^+H^-)$) bond dissociation energies display the fastest reaction rates. These results indicate that hydrogen abstraction from substrate, either in the form of hydride or hydrogen atom, is involved in the rate-determining step of reactions of H_{peroxo}.

Class III Reactions

Reactions of H_{peroxo} and Q with Class III substrates display a hyperbolic dependence on substrate concentration typical of classical enzyme kinetic mechanisms. For these substrates, binding is rate-determining at low substrate concentration but C–H activation chemistry is rate-determining at high substrate concentration. These substrates include propionaldehyde (Figure 4), acetaldehyde (Figure S6a), nitromethane (Figure S7a), sodium formate (Figure S8a), and acetonitrile (Figure 6) for H_{peroxo}, and nitromethane (Figure S7b) and acetonitrile (Figure S9) for Q (Table 5). Data belonging to this class follow the behavior described by eq 2 and can be fit to eq 3, where k_{obs} is the

$$I + S \underset{k_{-1}}{\overset{k_1}{\rightleftharpoons}} IS \xrightarrow{k_{sat}} H_{ox} + S_{ox} \quad (2)$$

$$k_{obs} - k_0 = \frac{k_{sat}[S]}{K_M + [S]} \quad (3)$$

observed rate constant at a defined substrate concentration, k_o is the rate constant of intermediate conversion in the absence of substrate, k_{sat} is defined in eq 2, and K_M is the apparent Michaelis constant describing the intermediate-substrate complex, defined as (k_{-1}+ k_{sat})/k_1.

For both H_{peroxo} and Q, all of the substrates that fit into Class III contain highly polarizable double bonds involving a heteroatom. The molecular dipole moments of these molecules are higher (>2.5 D) than those of Class I and Class II substrates (Table 1). This property provides a means by which these substrates can participate in dipole-induced interactions with protein amide bonds and polar side chains that line the hydrophobic cavities leading from the protein exterior to the active site. Whereas H^{peroxo} displays Class III behavior with substrates having D > ~2.5, Q displays only Class II behavior with the two substrates for which D > ~3.5. These findings reinforce the conclusion that the mechanisms by which H_{peroxo} and Q interact with substrates differ. The results also provide some guidance for predicting the behavior of a given substrate.

The values of k_{sat} provide a direct measure of the C–H bond activation step for the substrates employed and can therefore be used to obtain information about the details of the reaction mechanism for the intermediate species. In addition, a comparison of k_{sat} values for H_{peroxo} Class III substrates reveals a correlation between the rate constant and the heterolytic and homolytic C–H bond strengths of the substrate (Table 6 and Figure 6).[2] Substrates with lower C–H bond strengths react more rapidly with H_{peroxo}, bolstering the argument that the rate-determining step in the reaction involves C–H bond cleavage.

Two substrates display Class III behavior for reaction with Q, acetonitrile and nitromethane (Table 5). The large, non-classical magnitudes of the isotope effects for reactions of Q with these substrates suggest that they proceed with extensive quantum mechanical tunneling through the transition state at both 4 °C and 20 °C (Table 7). Although the two substrates are expected to exhibit both primary and secondary isotope effects, secondary effects should lie within semi-classical limits (< ~7). The large effects observed are therefore likely to be dominated by primary effects arising from hydrogen atom tunneling (43). The significant temperature dependence of the observed KIEs, which are larger at lower temperatures, also necessitates involvement of H-atom tunneling as defined by semi-classical transition state theory. This model predicts that both zero point energy considerations and hydrogen tunneling effects lead to a smaller free energy for hydrogen than for deuterium in a temperature-dependent manner (43, 44). Similar effects were previously observed for methane (23, 45).

For reactions with Q, there is no correlation of k_{sat} with the reported C–H bond activation energies; acetonitrile and nitromethane have similar homolytic and heterolytic BDEs but

[2]According to this hypothesis, the value of k_{sat} for reaction of CH_3CH_2CHO with H_{peroxo} is expected to be larger than that of all other substrates examined, but was slightly smaller than that for CH_3CHO. This result does not necessarily negate the conclusion that a trend between reaction rate and C–H bond strength exists because propionaldehyde is expected to react at its methyl group in addition to its aldehydic position, for which the C–H bond strengths are compared. Reactivity at multiple sites having different C–H bond strengths partially invalidates the comparison for this substrate.

display a 62–fold difference in their reaction rates with Q at 4 °C, acetonitrile reacting much more rapidly than nitromethane. Similarly, the rate constants do not correlate with the pK_a values or ionization potentials (IPs) of the substrates (Table 7). These results suggest that classical hydrogen atom transfer or hydride transfer featuring no quantum tunneling effects, proton transfer, and/or electron transfer from the substrate to the oxygenated diiron core are not determinants in the rate-determining step in the reaction mechanism. However, the observation that extensive quantum mechanical tunneling is operative in the reaction mechanism of Q (vide supra) suggests that C–H bond activation could be rate-determining via a non-classical mechanism. Differential contributions of quantum tunneling to the overall reaction processes for the two substrates could therefore lead to the observed effects.

Implications for the Reaction Mechanisms of H_{peroxo} and Q

The data presented here suggest that the mechanisms by which H_{peroxo} and Q react with substrate differ in both the nature of the C–H bond breaking process and the physical interaction with the substrate. Although reactions of H_{peroxo} seem to proceed by a classical hydrogen atom or hydride transfer mechanism, those of Q involve extensive non-classical character. Substrates with lower C–H bond strengths react preferentially with H_{peroxo}, although there is no correlation between bond energy and Q reaction rates, most likely because of non-classical character involving the latter. This conclusion is especially evident from inspection of Table 8, which compares the second-order rate constants for the *overall* reactions to substrate C–H bond strengths. For Class I and II substrates, the rate constants provided in Table 8 were determined by fitting the data to eq 1. For Class III substrate reactions, the rate constants were measured by fitting the linear portion of the curves at low substrate concentration to eq 1 to obtain a second-order value (k_{init} in Table 5).

The second-order rate constants provided in Table 8 account for all processes involved in the reactions, including substrate binding and C–H bond activation. Therefore, a direct comparison of rate constants to thermodynamic parameters is inappropriate given that the rate-determining steps of the reactions can differ among the substrates employed. A comparison of the *ratio* of the rate constants for reaction with H_{peroxo} and Q normalizes the substrate binding contributions in the limit that the binding affinities for the H_{peroxo} and Q protein complexes are the same for a given substrate. It is clear that, for some substrates, this situation does not obtain since these substrates belong to different classes of reactions with H_{peroxo} and Q. However, the presence of a clear correlation between the rate constant ratio and the C–H bond strength (vide infra) justifies the approximation.

A comparison of the ratio of the second-order rate constants for H_{peroxo} and Q reactions with the heterolytic and homolytic C–H bond strengths of the substrates clearly reveals an inverse trend between these parameters (Table 8). Substrates with weak C–H bonds are characterized by large rate constant ratios, consistent with substrates having weak C–H bonds preferentially reacting with H_{peroxo} vs. Q. Given this trend in reaction rate with C–H bond strength, it is understandable why methane, with high heterolytic and homolytic bond strengths of 312.2 kcal/mol (46) and 104.0 kcal/mol (47), respectively, reacts rapidly with Q but not at all with H_{peroxo}.

One major difference between the reactions of H_{peroxo} and Q with hydrocarbons is that large kinetic isotope effects, implicating hydrogen atom tunneling, are observed for Q but not H_{peroxo} for both Class II and Class III substrates.[3] In all cases the KIEs observed for reaction

[3]The KIE value for reaction of H_{peroxo} with CH_3NO_2 could not be determined, because reaction with CD_3NO_2 depends linearly on substrate concentration but the protio analogue displays Class III saturation behavior. A similar phenomenon was observed for reaction of this substrate with Q at 20 °C and was attributed to a difference in the rate-determining step for the protio and deutero substrates in Baik. M.-H., Newcomb, M., Friesner, R. A., and Lippard, S. J. (2003). *Chem. Rev. 103*, 2385-2419.

with H_{peroxo} were within the semiclassical limit (< ~7), suggesting that quantum mechanical tunneling does not play a role in the reaction mechanism. This finding also sheds light on the lack of reactivity of H_{peroxo} with methane. Because methane is kinetically stable, a large barrier height for its reaction is expected. For Q, tunneling across this barrier leads to progression along the reaction coordinate; for H_{peroxo}, no tunneling is involved, the barrier is too high to penetrate, and the reaction cannot proceed.

Reactions of H_{peroxo} with CH_3CN

The inverse isotope effect observed for reaction of CH_3CN with H_{peroxo} (Table 5 and Figure 5) is unexpected and suggests a distinctive reaction mechanism for this substrate. Because the sole oxidation product is glycolonitrile (48), the mechanism necessarily involves C–H bond activation. This reaction could occur by hydrogen atom abstraction to form a radical that recombines with a hydroxyl radical to form the hydroxylated product, by hydride abstraction to form a carbocation that is attacked by hydroxide, or by proton abstraction to form a carbanion that undergoes electrophilic addition with an electron-deficient group. All three of these mechanisms could potentially provide sufficient driving force for peroxide O–O bond cleavage and hydrocarbon oxidation.

The magnitude of the observed isotope effect (k_H/k_D) represents the product of primary and secondary contributions to the rate-determining step of the reaction. Primary contributions are expected to yield normal KIEs whereas secondary effects can be inverse or normal depending on the nature of the transition state. The inverse nature and relatively large magnitude of the KIE measured for the reaction of H_{peroxo} with CH_3CN indicates a significant involvement of secondary effects. Inverse secondary KIEs are caused by an increase in the out-of-plane bending force constant of the heavy isotope that may result from sp^2 to sp^3 rehybridization in the transition state (49). Secondary KIEs arising from this type of mechanism typically range from 0.8 to 0.9 (49), consistent with the observed value of 0.77. On the basis of these results we therefore propose a reaction mechanism in which acetonitrile is first deprotonated to form the cyanomethide anion, the structure of which involves significant sp^2 character at the α-carbon atom (50). This species can then attack, in a nucleophilic manner, an electrophilic oxygen atom of the iron-bound (hydro)peroxide resulting in the sp^3-hybridized product and the O–O bond is cleaved to form the oxidized product, glycolonitrile (Scheme 3).

Formation of a radical intermediate is not expected, because such a mechanism would not involve significant rehybridization at carbon and would therefore lead to a small and normal secondary kinetic isotope effect (43, 49, 51). For the same reason, hydride abstraction is also expected to produce a small and normal KIE. We therefore favor the mechanism proposed in Scheme 3. Similar conclusions were reached in a related study probing the mechanism of [1,1-$^2H_2$]nitroethane anion oxidation by D-amino acid oxidase (52).

The proposed reaction mechanism necessarily involves deprotonation of the acetonitrile molecule and formation of the cyanomethide anion prior to the rate-determining step. Although the pK_a of acetonitrile is ~25 (49), this value is most likely reduced by coordination to transition metals, which behave as Lewis acids. Additionally, the cyanomethide anion can be readily generated via deprotonation of acetonitrile by a strong base (53). These results imply that H_{peroxo} is highly basic. Indeed, we recently provided evidence that this peroxide moiety acquires a proton during conversion to Q, an event that leads to O–O bond cleavage, a necessary step for reaction with substrate (7).

In light of the proposed carbocation-based mechanism for reaction of H_{peroxo} with diethyl ether (Scheme 2b), these results were surprising. A mechanism in which a diiron(III) peroxide moiety undergoes electrophilic attack on the substrate carbanion in the rate-

determining step to account for the inverse secondary isotope effect seems to contradict the finding that C–H bond activation is rate-determining for diethyl ether and the other substrates employed in the study. Nevertheless, we favor such a mechanism and argue that, because k_{sat} for acetonitrile is very slow, the reaction pathway could differ significantly from that of diethyl ether and other much more rapidly reacting substrates. The large heterolytic C–H bond energy of acetonitrile disfavors formation of an intermediate carbocation via hydride abstraction. Presumably the favored mechanism is a consequence of the slow reactivity of this substrate.

When considered together, the two distinct two-electron mechanisms proposed for reaction of H_{peroxo} with diethyl ether vs acetonitrile are interesting. The results indicate (i) that H_{peroxo} prefers two-electron rather than one-electron transfer mechanisms and (ii) that H_{peroxo} is an electrophilic oxidant.

Implications for Other Systems with Multiple Oxidizing Species

The observation from this work and others (20, 26) that H_{peroxo} can oxidize organic substrates contributes to a growing body of evidence that two oxidants are operative in MMOH. Because the metabolic capabilities of methanotrophic organisms are restricted to the C_1 growth substrates methane and methanol, it is likely that the reactivity of H_{peroxo} is an adventitious result of being on the pathway of formation of Q, a potent methane oxidant. However, given the ability of H_{peroxo} to effect hydroxylation and epoxidation reaction chemistry, it is possible that some of the bioremediaton applications of the sMMO system, such as removal of trichloroethylene from polluted groundwater (3), arise from its activity.

Similar evidence for two oxidizing species has been provided for the hydrocarbon reactive, O_2-activating cytochrome P450 enzymes, which contain heme-iron active sites. The results of numerous studies employing kinetic isotope measurements and product analyses of wild-type and mutant enzyme reactions indicate the presence of a second electrophilic oxidant in addition to CpdI, the well-established Fe(IV)=O porphyrin cation radical species (54-62). The observed behavior is thought to arise from reactivity of a peroxo- and/or hydroperoxo-iron(III) species, similar in electronic arrangement to H_{peroxo}, which form after reaction of ferrous enzyme with O_2 and one electron. The mechanism proposed here for the reaction of H_{peroxo} with CH_3CN provides a benchmark for calibrating mechanisms imparted by iron peroxide species in the P450 as well as other enzyme systems.

CONCLUDING REMARKS

The present study conclusively demonstrates that both H_{peroxo} and Q react with substrates in the soluble methane monooxygenase system. Although both species are capable of performing oxidation reactions, they do so by distinct mechanisms. Reactions with Q involve extensive H-atom tunneling and with significant radical character, whereas reactions with electrophilic H_{peroxo} intermediate dot no invoke tunneling and seem to occur by two-electron carbocation or carbanion-based mechanisms.

Supplementary Material

Refer to Web version on PubMed Central for supplementary material.

Acknowledgments

We thank Dr. L. G. Beauvais, Dr. R. K. Behan, and Ms. W. J. Song for helpful discussions.

REFERENCES

1. Merkx M, Kopp DA, Sazinsky MH, Blazyk JL, Müller J, Lippard SJ. Dioxygen Activation and Methane Hydroxylation by Soluble Methane Monooxygenase: A Tale of Two Irons and Three Proteins. Angew. Chem. Int. Ed. 2001; 40:2782–2807.
2. Colby J, Stirling DI, Dalton H. The Soluble Methane Mono-oxygenase of *Methylococcus capsulatus* (Bath): Its Ability to Oxygenate *n*-Alkanes, *n*-Alkenes, Ethers, and Alicyclic, Aromatic and Heterocyclic Compounds. Biochem. J. 1977; 165:395–402. [PubMed: 411486]
3. Fox BG, Borneman JG, Wackett LP, Lipscomb JD. Haloalkene Oxidation by the Soluble Methane Monooxygenase from *Methylosinus trichosporium* OB3b: Mechanistic and Environmental Implications. Biochemistry. 1990; 29:6419–6427. [PubMed: 2207083]
4. Green J, Dalton H. Substrate Specificity of Soluble Methane Monooxygenase. Mechanistic Implications. J. Biol. Chem. 1989; 264:17698–17703. [PubMed: 2808342]
5. Liu KE, Johnson CC, Newcomb M, Lippard SJ. Radical Clock Substrate Probes and Kinetic Isotope Effect Studies of the Hydroxylation of Hydrocarbons by Methane Monooxygenase. J. Am. Chem. Soc. 1993; 115:939–947.
6. Brazeau BJ, Lipscomb JD. Kinetics and Activation Thermodynamics of Methane Monooxygenase Compound Q Formation and Reaction with Substrates. Biochemistry. 2000; 39:13503–13515. [PubMed: 11063587]
7. Tinberg C, Lippard SJ. Revisiting the Mechanism of Dioxygen Activation in Soluble Methane Monooxygenase from *M. capsulatus* (Bath): Evidence for a Multi-Step, Proton-Dependent Reaction Pathway. Biochemistry. 2009; 48:12145–12158. [PubMed: 19921958]
8. Liu KE, Valentine AM, Wang D, Huynh BH, Edmondson DE, Salifoglou A, Lippard SJ. Kinetic and Spectroscopic Characterization of Intermediates and Component Interactions in Reactions of Methane Monooxygenase from *Methylococcus capsulatus* (Bath). J. Am. Chem. Soc. 1995; 117:10174–10185.
9. Lee S-K, Lipscomb JD. Oxygen Activation Catalyzed by Methane Monooxygenase Hydroxylase Component: Proton Delivery during the O—O Bond Cleavage Steps. Biochemistry. 1999; 38:4423–4432. [PubMed: 10194363]
10. Broadwater JA, Ai J, Loehr TM, Sanders-Loehr J, Fox BG. Peroxodiferric Intermediate of Stearoyl-Acyl Carrier Protein Δ^9 Desaturase: Oxidase Reactivity during Single Turnover and Implications for the Mechanism of Desaturation. Biochemistry. 1998; 37:14664–14671. [PubMed: 9778341]
11. Moënne-Loccoz P, Baldwin J, Ley BA, Loehr TM, Bollinger JM Jr. O_2 Activation by Non-Heme Diiron Proteins: Identification of a Symmetric μ-1,2-Peroxide in a Mutant of Ribonucleotide Reductase. Biochemistry. 1998; 37:14659–14663. [PubMed: 9778340]
12. Moënne-Loccoz P, Krebs C, Herlihy K, Edmondson DE, Theil EC, Huynh BH, Loehr TM. The Ferroxidase Reaction of Ferritin Reveals a Diferric μ-1,2 Bridging Peroxide Intermediate in Common with Other O_2-Activating Non-Heme Diiron Proteins. Biochemistry. 1999; 38:5290–5295. [PubMed: 10220314]
13. Skulan AJ, Brunold TC, Baldwin J, Saleh L, Bollinger JM Jr. Solomon EI. Nature of the Peroxo Intermediate of the W48F/D84E Ribonucleotide Reductase Variant: Implications for O_2 Activation by Binuclear Non-Heme Iron Enzymes. J. Am. Chem. Soc. 2004; 126:8842–8855. [PubMed: 15250738]
14. Vu VV, Emerson JP, Martinho M, Kim YS, Münck E, Park MH, Que L Jr. Human Deoxyhypusine Hydroxylase, an Enzyme Invovled in Regulating Cell Growth, Activates O_2 with a Nonheme Diiron Center. Proc. Natl. Acad. Sci. USA. 2009; 106:14814–14819. [PubMed: 19706422]
15. Han W-G, Noodleman L. Structural Model Studies for the Peroxo Intermediate P and the Reaction Pathway from P → Q of Methane Monooxygenase Using Broken-Symmetry Density Functional Calculations. Inorg. Chem. 2008; 47:2975–2986. [PubMed: 18366153]
16. Gherman BF, Baik M-H, Lippard SJ, Friesner RA. Dioxygen Activation in Methane Monooxygenase: A Theoretical Study. J. Am. Chem. Soc. 2004; 126:2978–2990. [PubMed: 14995216]

17. Rinaldo D, Philipp DM, Lippard SJ, Friesner RA. Intermediates in Dioxygen Activation by Methane Monooxygenase: A QM/MM Study. J. Am. Chem. Soc. 2007; 129:3135–3147. [PubMed: 17326634]
18. Siegbahn PEM. O—O Bond Cleavage and Alkane Hydroxylation in Methane Monooxygenase. J. Biol. Inorg. Chem. 2001; 6:27–45. [PubMed: 11191221]
19. Lee S-K, Nesheim JC, Lipscomb JD. Transient Intermediates of the Methane Monooxygenase Catalytic Cycle. J. Biol. Chem. 1993; 268:21569–21577. [PubMed: 8408008]
20. Valentine AM, Stahl SS, Lippard SJ. Mechanistic Studies of the Reaction of Reduced Methane Monooxygenase Hydroxylase with Dioxygen and Substrates. J. Am. Chem. Soc. 1999; 121:3876–3887.
21. Liu KE, Wang D, Huynh BH, Edmondson DE, Salifoglou A, Lippard SJ. Spectroscopic Detection of Intermediates in the Reaction of Dioxygen with Reduced Methane Monooxygenase Hydroxylase from *Methylococcus capsulatus* (Bath). J. Am. Chem. Soc. 1994; 116:7465–7466.
22. Shu L, Nesheim JC, Kauffmann K, Münck E, Lipscomb JD, Que L Jr. An $Fe_2^{IV}O_2$ Diamond Core Structure for the Key Intermediate Q of Methane Monooxygenase. Science. 1997; 275:515–518. [PubMed: 8999792]
23. Ambundo EA, Friesner RA, Lippard SJ. Reactions of Methane Monooxygenase Intermediate Q with Derivatized Methanes. J. Am. Chem. Soc. 2002; 124:8770–8771. [PubMed: 12137510]
24. Lee S-K, Fox BG, Froland WA, Lipscomb JD, Münck E. A Transient Intermediate of the Methane Monooxygenase Catalytic Cycle Containing an $Fe^{IV}Fe^{IV}$ Cluster. J. Am. Chem. Soc. 1993; 115:6450–6451.
25. Baik M-H, Gherman BF, Friesner RA, Lippard SJ. Hydroxylation of Methane by Non-Heme Diiron Enzymes: Molecular Orbital Analysis of C-H Bond Activation by Reactive Intermediate Q. J. Am. Chem. Soc. 2002; 124:14608–14615. [PubMed: 12465971]
26. Beauvais LG, Lippard SJ. Reactions of the Peroxo Intermediate of Soluble Methane Monooxygenase Hydroxylase with Ethers. J. Am. Chem. Soc. 2005; 127:7370–7378. [PubMed: 15898785]
27. Andersson KK, Froland WA, Lee S-K, Lipscomb JD. Dioxygen Independent Oxygenation of Hydrocarbons by Methane Monooxygenase Hydroxylase Component. New J. Chem. 1991; 15:411–415.
28. Jiang Y, Wilkins PC, Dalton H. Activation of the Hydroxylase of sMMO from *Methylococcus capsulatus* (Bath) by Hydrogen Peroxide. Biochim. Biophys. Acta. 1993; 1163:105–112. [PubMed: 8476925]
29. Brazeau BJ, Austin RN, Tarr C, Groves JT, Lipscomb JD. Intermediate Q from Soluble Methane Monooxygenase Hydroxylates the Mechanistic Substrate Probe Norcarane: Evidence for a Stepwise Reaction. J. Am. Chem. Soc. 2001; 123:11831–11837. [PubMed: 11724588]
30. Choi S-Y, Eaton PE, Kopp DA, Lippard SJ, Newcomb M, Shen R. Cationic Species Can Be Produced in Soluble Methane Monooxygenase-Catalyzed Hydroxylation Reactions; Radical Intermediates Are Not Formed. J. Am. Chem. Soc. 1999; 121:12198–12199.
31. Newcomb M, Shen R, Lu Y, Coon MJ, Hollenberg PF, Kopp DA, Lippard SJ. Evaluation of Norcarane as a Probe for Radicals in Cytochrome P450- and Soluble Methane Monooxygenase-Catalyzed Hydroxylation Reactions. J. Am. Chem. Soc. 2002; 124:6879–6886. [PubMed: 12059209]
32. Ruzicka F, Huang D-S, Donnelly MI, Frey PA. Methane Monooxygenase Catalyzed Oxygenation of 1,1-Dimethylcyclopropane. Evidence for Radical and Carbocationic Intermediates. Biochemistry. 1990; 29:1696–1700. [PubMed: 2331458]
33. Coufal DE, Blazyk JL, Whittington DA, Wu WW, Rosenzweig AC, Lippard SJ. Sequencing and Analysis of the *Methylococcus capsulatus* (Bath) Soluble Methane Monooxygenase Genes. Eur. J. Biochem. 2000; 267:2174–2185. [PubMed: 10759840]
34. Kopp DA, Gassner GT, Blazyk JL, Lippard SJ. Electron-Transfer Reactions of the Reductase Component of Soluble Methane Monooxygenase from *Methylococcus capsulatus* (Bath). Biochemistry. 2001; 40:14932–14941. [PubMed: 11732913]

35. Beauvais LG, Lippard SJ. Reactions of the Diiron(IV) Intermediate Q in Soluble Methane Monoxygenase with Fluoromethanes. Biochem. Biophys. Res. Commun. 2005; 338:262–266. [PubMed: 16176805]
36. Muthusamy M, Ambundo EA, George SJ, Lippard SJ, Thorneley RNF. Stopped-Flow Fourier Transform Infrared Spectroscopy of Nitromethane Oxidation by the Diiron(IV) Intermediate of Methane Monooxygenase. J. Am. Chem. Soc. 2003; 125:11150–11151. [PubMed: 16220908]
37. Lee S-K, Nesheim JC, Lipscomb JD. Transient Intermediates of the Methane Monooxygenase Catalytic Cycle. J. Biol. Chem. 1993; 268:21569–21577. [PubMed: 8408008]
38. Lippard SJ. Hydroxylation of C-H Bonds at Carboxylate-Bridged Diiron Centers. Phil. Trans. R. Soc. A. 2005; 363:861–877. [PubMed: 15901540]
39. Brazeau BJ, Lipscomb JD. Key Amino Acid Residues in the Regulation of Soluble Methane Monooxygenase Catalysis by Component B. Biochemistry. 2003; 42:5618–5631. [PubMed: 12741818]
40. Rosenzweig AC, Frederick CA, Lippard SJ, Nordlund P. Crystal Structure of a Bacterial Non-Haem Iron Hydroxylase that Catalyses the Biological Oxidation of Methane. Nature. 1993; 366:537–543. [PubMed: 8255292]
41. Gherman BF, Lippard SJ, Friesner RA. Substrate Hydroxylation in Methane Monooxygenase: Quantitative Modeling via Mixed Quantum Mechanics/Molecular Mechanics Techniques. J. Am. Chem. Soc. 2005; 127:1025–1037. [PubMed: 15656641]
42. Zheng H, Lipscomb JD. Regulation of Methane Monooxygenase Catalysis Based on Size Exclusion and Quantum Tunneling. Biochemistry. 2006; 45:1685–1692. [PubMed: 16460015]
43. Sühnel, J.; Schowen, RL. Theoretical Basis for Primary and Secondary Hydrogen Isotope Effects. In: Cook, PF., editor. Enzyme Mechanism from Isotope Effects. CRC Press; Boca Raton, FL: 1991. p. 3-36.
44. Pu J, Gao J, Truhlar DJ. Multidimensional Tunneling, Recrossing, and the Transmission Coefficient for Enzymatic Reactions. Chem. Rev. 2006; 106:3140–3169. [PubMed: 16895322]
45. Nesheim JC, Lipscomb JD. Large Kinetic Isotope Effects in Methane Oxidation Catalyzed by Methane Monooxygenase: Evidence for C—H Bond Cleavage in a Reaction Cycle Intermediate. Biochemistry. 1996; 35:10240–10247. [PubMed: 8756490]
46. Screttas CG. Some Properties of Heterolytic Bond Dissociation Energies and Their Use as Molecular Parameters for Rationalizing or Predicting Reactivity. J. Org. Chem. 1980; 45:333–336.
47. Luo, Y-R. Comprehensive Handbook of Chemical Bond Energies. CRC Press; Boca Raton, FL: 2007.
48. Stahl SS, Francisco WA, Merkx M, Klinman JP, Lippard SJ. Oxygen Kinetic Isotope Effects in Soluble Methane Monooxygenase. J. Biol. Chem. 2001; 276:4549–4553. [PubMed: 11073959]
49. Anslyn, EV.; Dougherty, DA. Modern Physical Organic Chemistry. University Science Books; Sausalito, CA: 2006.
50. Moran S, Ellis HB Jr. DeFrees DJ, McLean AD, Ellison GB. Carbanion Spectroscopy: CH_2CN^- J. Am. Chem. Soc. 1987; 109:5996–6003.
51. Hanzlik RP, Shearer GO. Transition State Structure for Peracid Epoxidation. Secondary Deuterium Isotope Effects. J. Am. Chem. Soc. 1975; 97:5231–5233.
52. Kurtz KA, Fitzpatrick PF. pH and Secondary Kinetic Isotope Effects on the Reaction of D-Amino Acid Oxidase with Nitroalkane Anions: Evidence for Direct Attack on the Flavin by Carbanions. J. Am. Chem. Soc. 1997; 119:1155–1156.
53. Rossi L, Feroci M, Inesi A. The Electrogenerated Cyanomethyl Anion in Organic Synthesis. Mini-Rev. Org. Chem. 2005; 2:79–90.
54. Jin S, Bryson TA, Dawson JH. Hydroperoxoferric Heme Intermediate as a Second Electrophilic Oxidant in Cytochrome P450-Catalyzed Reactions. J. Biol. Inorg. Chem. 2004; 9:644–653. [PubMed: 15365901]
55. Jin S, Makris TM, Bryson TA, Sligar SG, Dawson JH. Epoxidation of Olefins by Hydroperoxo-Ferric Cytochrome P450. J. Am. Chem. Soc. 2003; 125:3406–3407. [PubMed: 12643683]
56. Newcomb M, Aebisher D, Shen R, Chandrasena REP, Hollenberg PF, Coon MJ. Kinetic Isotope Effects Implicate Two Electrophilic Oxidants in Cytochrome P450-Catalyzed Hydroxylations. J. Am. Chem. Soc. 2003; 125:6064–6065. [PubMed: 12785830]

57. Newcomb M, Hollenberg PF, Coon MJ. Multiple Mechanisms and Multiple Oxidants in P450-Catalyzed Hydroxylations. Arch. Biochem. Biophys. 2003; 409:72–79. [PubMed: 12464246]
58. Sheng X, Zhang H, Hollenberg PF, Newcomb M. Kinetic Isotope Effects in Hydroxylation Reactions Effected by Cytochrome P450 Compounds I Implicate Multiple Electrophilic Oxidants for P450-Catalyzed Oxidations. Biochemistry. 2009; 48:1620–1627. [PubMed: 19182902]
59. Vatsis KP, Coon MJ. *Ipso*-Substitution by Cytochrome P450 with Conversion of *p*-Hydroxybenzene Derivatives to Hydroquinone: Evidence for Hydroperoxo-Iron As the Active Oxygen Species. Arch. Biochem. Biophys. 2002; 397:119–129. [PubMed: 11747318]
60. Vaz ADN, McGinnity DF, Coon MJ. Epoxidation of Olefins by Cytochrome P450: Evidence from Site-Specific Mutagenesis for Hydroperoxo-Iron as an Electrophilic Oxidant. Proc. Natl. Acad. Sci. USA. 1998; 95:3555–3560. [PubMed: 9520404]
61. Vaz ADN, Pernecky SJ, Raner GM, Coon MJ. Peroxo-Iron and Oxenoid-Iron Species as Alternative Oxygenating Agents in Cytochrome P450-Catalyzed Reactions: Switching by Threonine-302 to Alanine Mutagenesis of Cytochrome P450 2B4. Proc. Natl. Acad. Sci. USA. 1996; 93:4644–4648. [PubMed: 8643457]
62. Volz TJ, Rock DA, Jones JP. Evidence for Two Different Active Oxygen Species in Cytochrome P450 BM3 Mediated Sulfoxidation and N-Dealkylation Reactions. J. Am. Chem. Soc. 2002; 124:9724–9725. [PubMed: 12175228]
63. CRC Handbook of Chemistry and Physics. 68 ed.. CRC Press, Inc.; Boca Raton, FL: 1987.
64. Halle LF, Klein FS, Beauchamp JL. Properties and Reactions of Organometallic Fragments in the Gas Phase. Ion Beam Studies of FeH^+ J. Am. Chem. Soc. 1984; 106:2543–2549.
65. Cheng J-P, Handoo KL, Parker VD. Hydride Affinities of Carbenium Ions in Acetonitrile and Dimethyl Sulfoxide Solution. J. Am. Chem. Soc. 1993; 115:2655–2660.
66. Gligorovski S, Herrmann H. Kinetics of Reactions of OH with Organic Carbonyl Compounds in Aqueous Solution. Phys. Chem. Chem. Phys. 2004; 6:4118–4126.
67. Gochel-Dupuis M, Delwiche J, Hubin-Franskin M-J, Collin JE. High-Resolution HeI Photoelectron Spectrum of Acetonitrile. Chem. Phys. Lett. 1992; 193:41–48.
68. Allam SH, Migahed MD, El Khodary A. Electron-Impact Study of Nitrobenzene and Nitromethane. Int. J. Mass Spectrom. Ion Phys. 1981; 39:117–122.

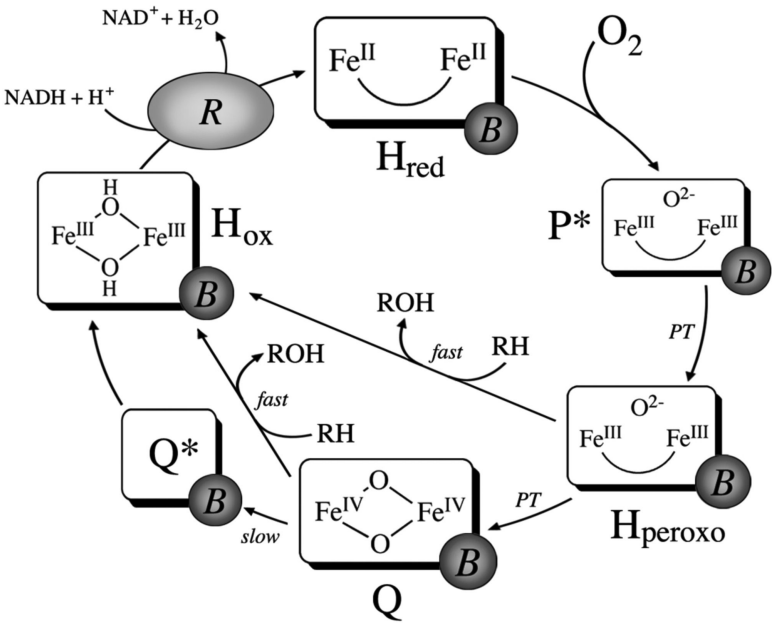

Scheme 1.
Current Working Model of Catalysis by the MMOH Diiron Center

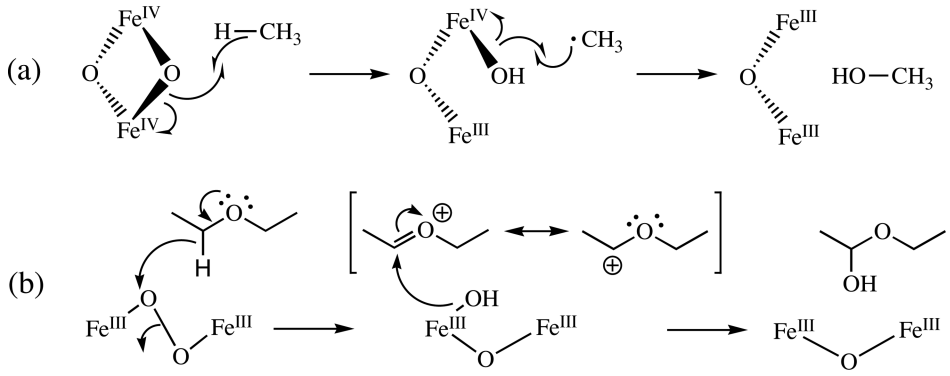

Scheme 2.

Proposed Mechanisms of Methane Hydroxylation by Q (a) and Diethyl Ether Oxidation by H_{peroxo} (b)

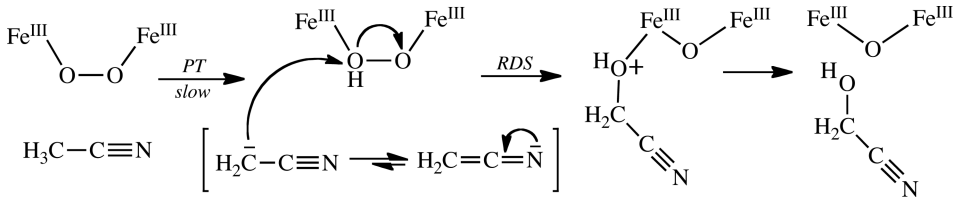

Scheme 3.
Proposed Mechanism of CH_3CN Hydroxylation by H_{peroxo}; RDS, rate-determining step.

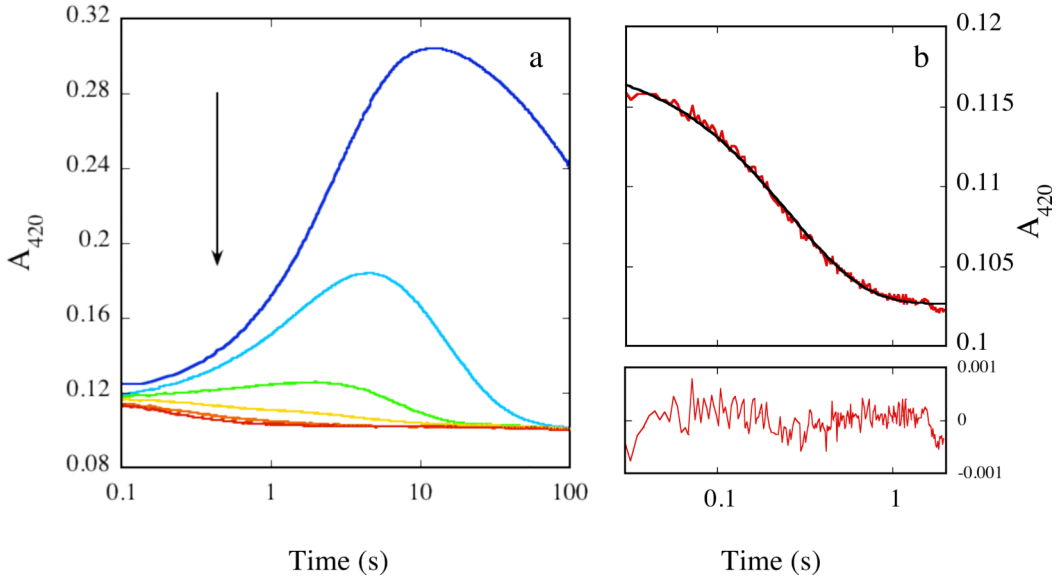

Figure 1.

(a) Representative absorbance profile for the reaction of 50 μM $MMOH_{red}$ with a mixture of excess O_2 and CH_3CH_2CHO in the presence of 2 equiv MMOB at 4 °C and 420 nm. [CH_3CH_2CHO] = 0 mM (blue), 5.8 mM (cyan), 24.9 mM (green), 69.7 mM (yellow), 122.3 mM (orange), and 214.9 mM (red). Data collected on separate occasions with different batches of protein yielded similar results. (b) Representative fit of data (red line) depicted in (a) collected in the presence of 214.9 mM CH_3CH_2CHO to a single exponential decay process (black line). Fit residuals are depicted below the plot.

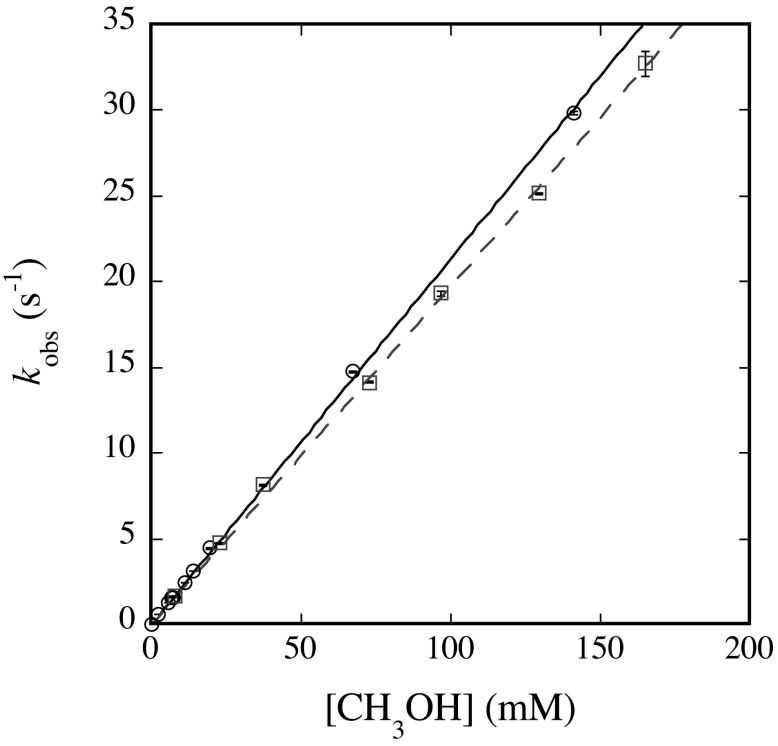

Fig. 2.

Plot of k_{obs} versus [CH_3OH] (circles, solid line) or [CD_3OH] (squares, dashed line) for reaction with Q at 4 °C and pH 7.0. 200 μM $MMOH_{red}$ and 400 μM MMOB were mixed rapidly with excess O_2, the reaction mixture was aged for 12 s, and then buffer containing the appropriate concentration of methanol was introduced. Data were analyzed as noted in the text. Error bars represent one standard deviation at the 95% confidence level.

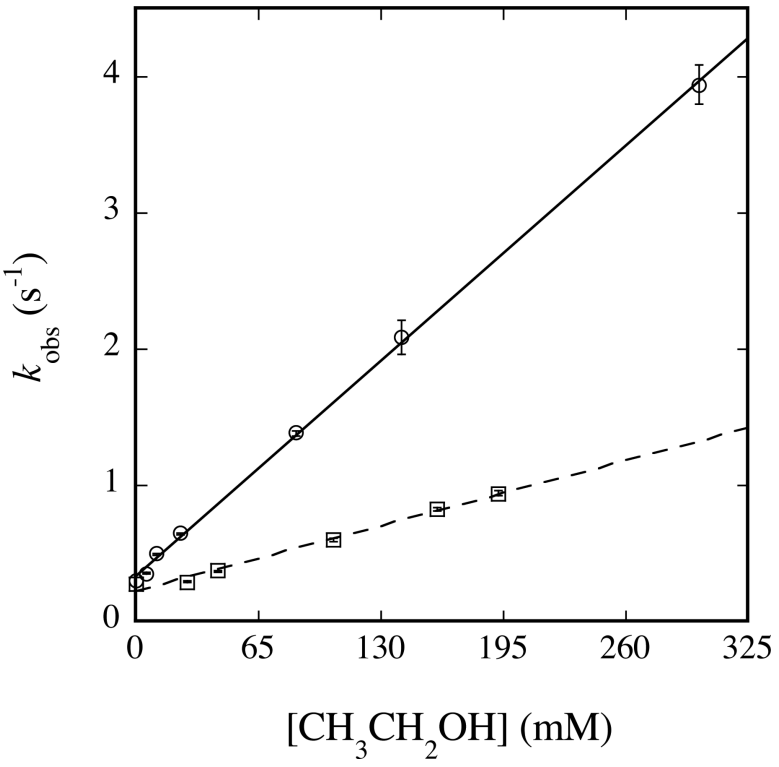

Fig. 3.

Plot of k_{obs} versus [CH_3CH_2OH] (circles, solid line) or [CD_3CD_2OH] (squares, dashed line) for reaction with H_{peroxo} at 4 °C and pH 7.0. 200 μM $MMOH_{red}$ and 400 μM MMOB were mixed rapidly with excess O_2, the reaction mixture was aged for 2 s, and then buffer containing the appropriate concentration of ethanol was introduced. Data were analyzed as noted in the text. Error bars represent one standard deviation at the 95% confidence level.

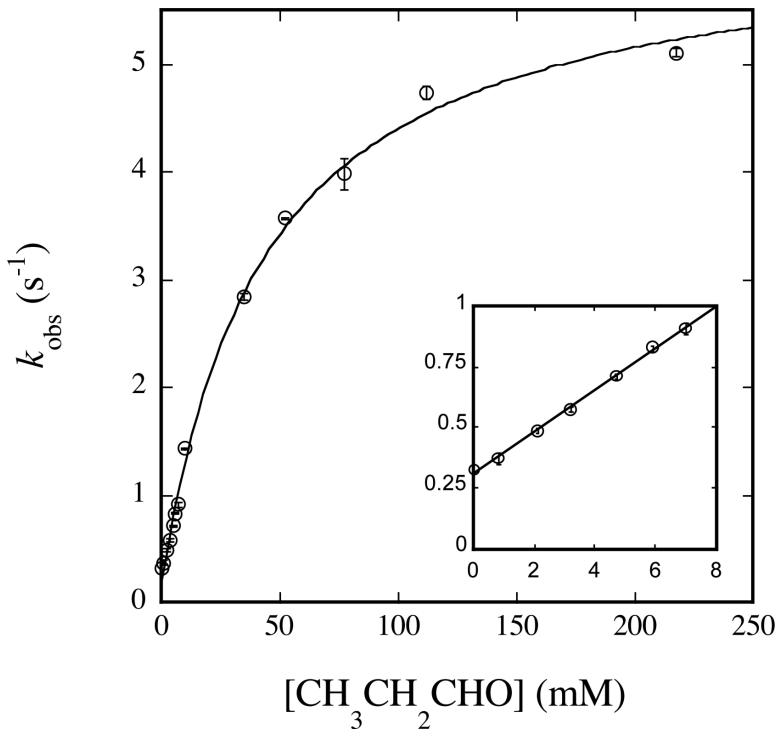

Fig. 4.

Plot of k_{obs} versus [CH_3CH_2CHO] for reaction with H_{peroxo} at 4 °C and pH 7.0. 50 μM $MMOH_{red}$ and 100 μM MMOB were mixed rapidly with excess O_2, the reaction mixture was aged for 2 s, and then buffer containing the appropriate concentration of propionaldehyde was introduced. Data were analyzed as noted in the text and fit to eq 3. Data collected at low [CH_3CH_2CHO] (k_{init}) is depicted in the inset. Error bars represent one standard deviation at the 95% confidence level.

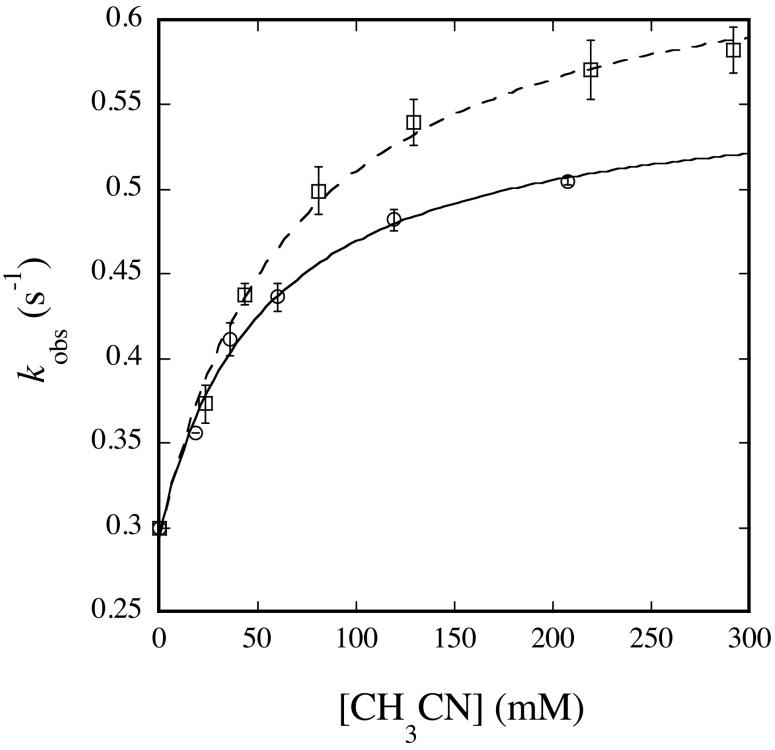

Fig. 5.

Plot of k_{obs} versus [CH_3CN] (circles, solid line) or [CD_3CN] (squares, dashed line) for reaction with H_{peroxo} at 4 °C and pH 7.0. 200 μM $MMOH_{red}$ and 400 μM MMOB were mixed rapidly with excess O_2, the reaction mixture was aged for 2 s, and then buffer containing the appropriate concentration of acetonitrile was introduced. Data were analyzed as noted in the text. Error bars represent one standard deviation at the 95% confidence level.

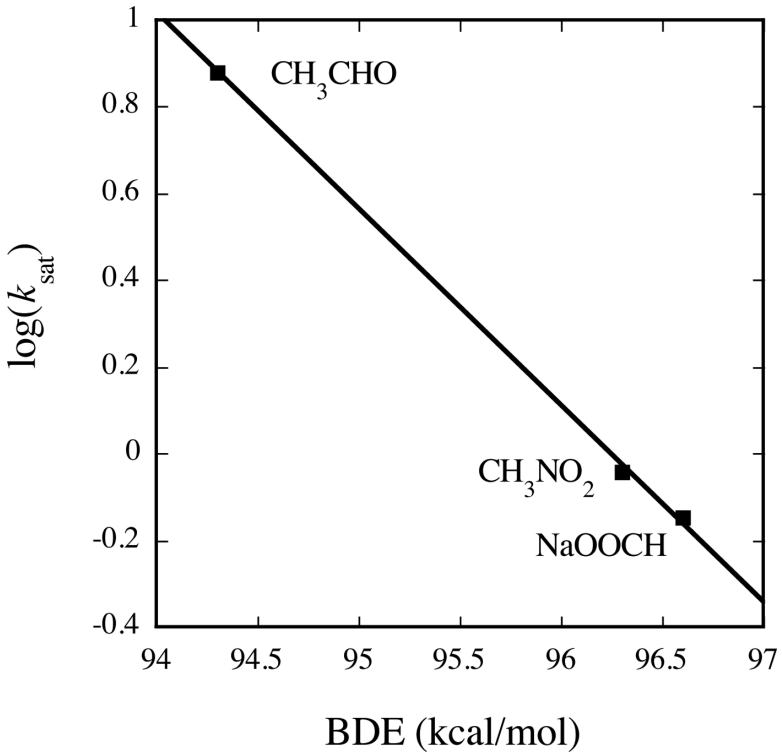

Fig. 6.

Linear inverse correlation between k_{sat} and C–H BDE for Class III substrates of H_{peroxo}. Reactions employed final concentrations of 50 μM MMOH and 100 μM MMOB and were performed at 4 °C and pH 7.0.

Table 1

Classification of Substrates

Substrate	Substrate Class (H_{peroxo})	Substrate Class (Q)	Dipole Moment (D)[a]
CH_4[b]	nr[c]	II	0
C_2H_6[d]	nd[e]	1	0
Et_2O[f]	II	II	1.10
HCOONa	III	nr[c]	1.41[g]
CH_3CH_2OH	II	I	1.69
CH_3OH	II	I	1.70
CH_3CH_2CHO	III	I or II[h]	2.52
CH_3CHO	III	II	2.69
CH_3NO_2	III	III	3.46
CH_3CN	III	III	3.92

[a] Data from (63).

[b] Data from (23).

[c] No reaction.

[d] Data from (39).

[e] Not determined.

[f] Data from (26).

[g] This value was determined for HCOOH but should approximate that of HCOONa.

[h] For CH_3CH_2CHO, the KIE was not determined but a linear dependence on substrate concentration was observed, designating this substrate as Class I or Class II.

Table 2

Rate Constants for Class I Substrates of Q

Substrate	k_{obs} (M^{-1} s^{-1})	KIE_{app}[a]
CH_3CH_2OH	35.7 ± 0.1	
CD_3CD_2OH	34 ± 3	1.05 ± 0.9
CH_3OH	218 ± 8	
CD_3OD	206 ± 16	1.06 ± 0.9

[a] Apparent kinetic isotope effect, k_H/k_D.

Table 3

Rate Constants for Class II Substrates of H_{peroxo}

Substrate	k_{obs} (M^{-1} s^{-1})	KIE_{app} [a]
$(CH_3CH_2)_2O$ [b]	17 ± 1	
$(CD_3CD_2)_2O$ [b]	8.7 ± 0.1	2.02 ± 0.2
CH_3CH_2OH	12.13 ± 0.01	
CD_3CD_2OH	3.93 ± 0.06	3.09 ± 0.05
CH_3OH	2.4 ± 0.6	
CD_3OD	1.54 ± 0.02	1.6 ± 0.4

[a] Apparent kinetic isotope effect, k_H/k_D.

[b] Data from (26).

Table 4

Class II Substrates of H_{peroxo}: Correlation Between k_{obs} and BDE

Substrate[a]	k_{obs} (M^{-1} s^{-1})	$D(R^+H^-)$ (kcal/mol)[b]	$-\Delta G_{hydride}(R^+)s$ (kcal/mol)[c]	D(RH) (kcal/mol)[d]
$(CH_3C\mathbf{H}_2)_2O$[e]	17 ± 1	214	94.8	93.0
$CH_3C\mathbf{H}_2OH$	12.13 ± 0.01	231.9	110.9	94.6
$C\mathbf{H}_3OH$	2.4 ± 0.6	255	131.8	96.06

[a] $D(R^+H^-)$ and D(RH) are given for the bolded C–H bond. For diethyl ether, this position is the sole C–H bond activated by sMMO in steady state assays (26).

[b] Data from (64).

[c] Calculated using $-\Delta G_{hydride}(R^+)s = 0.904D(R^+H^-) - 98.7$ kcal/mol from (65). This relationship was originally derived for aromatic molecules in acetonitrile and DMSO, but should provide a good approximation for non-aromatic systems in aqueous solution.

[d] Data from (47).

[e] Data from (26).

Table 5

Class III Substrates of H_{peroxo} and Q

Substrate	Species	k_{sat} (s^{-1})	K_M (mM)	k_{init} (M^{-1} s^{-1})[a]	KIE_{app}[b]
CH_3CH_2CHO	H_{peroxo}	6.0 ± 0.2	44 ± 4	85.5 ± 0.1	nd[c]
CH_3CHO	H_{peroxo}	7.6 ± 0.2	43 ± 3	110.08 ± 0.03	nd[c]
HCOONa	H_{peroxo}	0.71 ± 0.01	458 ± 65	0.91 ± 0.01	nd[c]
CH_3CN	H_{peroxo}	0.2727 ± 0.0003	39 ± 6	2.93 ± 0.01	
CD_3CN	H_{peroxo}	0.352 ± 0.001	78 ± 3	2.02	0.775 ± 0.002
CH_3NO_2	H_{peroxo}	0.912 ± 0.002	403 ± 11	nd[c]	na[d]
CH_3CN	Q	126 ± 8	617 ± 71	180 ±1	
CD_3CN	Q	2.02 ± 0.03	130 ± 3	12.4	62 ± 4
CH_3NO_2	Q	1.54 ± 0.2	13 ± 1	nd[c]	
CD_3NO_2	Q	0.005 ± 0.0005	11 ± 5	nd[c]	31 ± 3

[a] k_{init} values were calculated by fitting the linear portion of the curve at low substrate concentration to eq 1.

[b] Apparent kinetic isotope effect, $k_{sat,H}/k_{sat,D}$.

[c] Not determined.

[d] Not applicable. For CD_3NO_2, KIE_{app} could not be determined for the reaction of H_{peroxo} because k_{obs} displayed a linear dependence on substrate concentration.

Table 6

Class III Substrates of H_{peroxo}: Correlation Between k_{obs} and BDE

Substrate[a]	k_{sat} (s^{-1})	D(R^+H^-) (kcal/mol)[b]	-$\Delta G_{hydride}$ (R^+)s (kcal/mol)[c]	D(RH) (kcal/mol)
$CH_3CH_2C\mathbf{H}O$	6.0 ± 0.2	224	103.8	87.5[f]
$CH_3C\mathbf{H}O$	7.6 ± 0.2	231.4	110.5	94.3[d]
$C\mathbf{H}_3NO_2$	0.912 ± 0.002	-	-	96.3[d]
HCOONa	0.71 ± 0.04	267[e]	142.7	96.6[d,e]

[a] $D(R^+H^-)$ and D(RH) are given for the bolded C–H bond.

[b] Data from (64).

[c] Calculated using -$\Delta G_{hydride}$ (R^+)s = 0.904$D(R^+H^-)$ – 98.7 kcal/mol from (65). This relationship was originally derived for aromatic molecules in acetonitrile and DMSO, but should provide a good approximation for non-aromatic systems in aqueous solution.

[d] Data from (47)

[e] These values were originally determined for HCOOH but should approximate that of HCOONa.

[f] Data from (66).

Table 7

Apparent KIEs and Correlation of k_{sat} with Thermodynamic Parameters for Class III Substrates of Q at 4 °C and °20 C

Substrate	T (°C)	k_{sat} (s^{-1})	KIE_{app} [a]	D(RH) (kcal/mol) [b]	IP (eV)	pK_a [c]
CH_3CN	4	126 ± 8		97.0	12.20 [d]	25.0
	20 [e]	282 ± 10				
CD_3CN	4	2.02 ± 0.03	62 ± 4			
	20 [e]	6.1 ± 0.1	46.4 ± 2.3			
CH_3NO_2	4	1.54 ± 0.02		96.3	11.28 [f]	10.2
	20 [e]	5.34 ± 0.02				
CD_3NO_2	4	0.050 ± 0.0005	31 ± 3			
	20 [e]	0.66 ± 0.2	8.1 ± 0.2			

[a] Apparent kinetic isotope effect, $k_{sat,H}/k_{sat,D}$.

[b] Data from (47).

[c] Data from (49).

[d] Data from (67).

[e] Data from (23).

[f] Data from (68).

Table 8

Comparison of Second-Order Rate Constants for Reactions of H_{peroxo} and Q with Substrates

Substrate[a]	Species	k_{obs} (M^{-1} s^{-1})[b]	k_{peroxo}/k_Q	$D(R^+H^-)$ (kcal/mol)[c]	$-\Delta G_{hydride}$ (R^+)s (kcal/mol)[d]	D(RH) (kcal/mol)
$(CH_3C\mathbf{H}_2)_2O$[e]	H_{peroxo}	17 ± 1				
	Q	2.2 ± 1	**7.7**	214	94.8	89.0[f]
$CH_3CH_2C\mathbf{H}O$	H_{peroxo}	85.5 ± 0.1				
	Q	14.10 ± 0.02	**6.06**	224	103.8	87.5[g]
$CH_3C\mathbf{H}O$	H_{peroxo}	110.08 ± 0.03				
	Q	81.7 ± 0.1	**1.35**	231.4	110.5	94.3[f]
$CH_3C\mathbf{H}_2OH$	H_{peroxo}	12.13 ± 0.01				
	Q	35.7 ± 0.1	**0.34**	231.9	110.9	94.6[f]
$C\mathbf{H}_3OH$	H_{peroxo}	2.4 ± 0.6				
	Q	218 ± 8	**0.011**	255	131.8	96.1[f]

[a] $D(R^+H^-)$ and D(RH) are given for the bolded C–H bond.

[b] Second-order rate constants for Class III substrates are given by the measured k_{init} values. Only Class III substrates for which k_{init} values were discretely measured by collecting >5 data points at low substrate concentration in the linear region of the curve are shown.

[c] Data from (64).

[d] Calculated using $-\Delta G_{hydride}$ (R^+)s = $0.904D(R^+H^-) - 98.7$ kcal/mol from (65). This relationship was originally derived for aromatic molecules in acetonitrile and DMSO, but should provide a good approximation for non-aromatic systems in aqueous solution.

[e] Data from (26).

[f] Data from (47).

[g] Data from (66).